LOW OZONE ANOMALIES IN THE WINTER MIDDLE STRATOSPHERE

G. L. Manney, L. Froidevaux, J. W. Waters, R. W. Zurek

Jet Propulsion Laboratory/California Institute of Technology

J. B. Kumer, J. L. Mergenthaler, A. E. Roche,

Lockheed Palo Alto Research Laboratory,

A, O'Neil],

Centre for Global Atmospheric Modelling, Reading UK,

R. Swinbank,

Meteorological Office, Bracknell UK

Submitted to

Journal of Geophysical Research, Atmospheres

August 1994

Abstract,

Microwave Limb Sounder observations of mid-stratospheric ozone during stratospheric warmings show tongues of high ozone drawn up from low latitudes into the developing anticyclone. Several days later, an isolated region of low ozone mixing ratios appears, centered in the anticyclone, and extending in the vertical from ≈15 to 5 hPa, with higher mixing ratios both above and below. These anomalous mixing ratios during northern hemisphere warmings are comparable to values well inside the vortex, and are typically ≈3 ppmv lower than normal mid-latitude extra-vortex mixing ratios. This type of feature is seen whenever the anticyclone is strong and persistent, including during relatively strong minor warmings in the southern hemisphere. Three-dimensional back trajectory calculations indicate that the air in the region of the ozone anomalies originates at higher altitudes and low latitudes, where ozone mixing ratios are much higher. The air parcels studied here are typically confined together for 1 to 3 weeks before the lowest ozone mixing ratios are observed. The trajectory calculations and comparisons with passive tracer data confirm that the observed ozone anomalies in the mid-stratosphere could not result solely from transport processes.

Introduction

The Microwave Limb Sounder (MLS) instrument on the Upper Atmosphere Research Satellite (UARS) bass been measuring ozone throughout the stratosphere since September 1991, through three northern hemisphere (NH) and three southern hemisphere (SH) winters [Froidevaux et al. 1994]. This provides a multi-year dataset of three-dimensional ozone fields, including measurements during many dynamically active periods in both hemispheres,

Strong stratospheric warmings are common throughout the NH winter [e.g., Andrews et al. 1987], and weaker warmings are common in early and late winter in the SH [e.g. Farrara et al. 1992, Manney et al, 1993]. During these events, the polar vortex is typically shifted off the pole and tongues of low latitude air are seen to be drawn into the polar regions from low latitudes [e.g., Manney et al. 1993, Manney et al, 1994a] in the mid-stratosphere. Planetary scale waves are generally strongest in the middle and upper stratosphere [Manney et al. 1991, Fishbein et al. 1993], so the distortion and displacement of the vortex is greatest there,

Examination of mid-stratospheric MLS ozone data during a number of stratospheric warmings reveals that while tongues of ozone rich air are drawn into the anticyclone from low latitudes during stratospheric warmings, this is followed by the formation of an isolated region of very low ozone in the anticyclone. We show here observed meteorological and ozone fields for several examples of this phenomenon. In addition, we use passive tracer data from MLS and the Cryogen Limb Array EtaIon Spectrometer (CLAES) on UARS, and calculations of air parcel trajectories to explore the origins of the air in these low ozone regions,

Data and Analysis

The ozone data are from the MLS 205 GHz radiometer; they have horizontal resolution of ≈400 km and intrinsic vertical resolution of ≈4 km, The UARS MLS instrument is described by Barath et al. [1993], the measurement technique by Waters [1993], and retrieval methods by Froidevaux et al. [1994]. Precision (rms) of individual ozone measurements for the altitudes examined here are ≈0.3 ppmv, with absolute accuracies of ≈5--15% [Froidevaux et al. 1994].

Passive tracer data include H_2O from MLS and N_2O and CH_4 from CLAES. The CLAES instrument is described by Roche et al. [1993]. An earlier version of the CLAES N_2O and CH_4 data is described by Kumer et al. [1993]. The data are still in the validation process; this process has verified that the data used here (v0007) are suitable for studies of morphology and regional variation. Typical precision and systematic error estimates for N_2O in the mid-stratosphere are (10 ppbv rms, 20%), and for CH_4 are (50 ppbv, 20%). The MLS H_20 data are described by Lahoz et al. [1994]. Single profile precision and accuracy estimates for H_2O are (0.3 ppmv, 15%) at 4.6 hPa [Lahoz et al. 1994]. Comparison of these passive tracer data with potential vorticity (PV) indicates that N_20 show the strongest correlation with PV during the time periods used here; we therefore focus more closely on N_20 than on the other tracers.

Both CLAES and MLS data have been mapped to a 4° latitude by 5° longitude grid, consistent with the general meridional resolution of both instruments. CLAES data are gridded by linearly interpolating data for a 24 h period to a regular latitude-longitude grid; ascending and descending orbit tracks are treated separately and then averaged. MLS data are gridded using Fourier transform techniques that separate time and longitude variations [Elson and Froidevaux 1993]. All data are interpolated to isentropic (θ) surfaces using United Kingdom Meteorological Office (UKMO) temperatures.

The trajectory code used here is described by Manney et al. [1994b]; it uses a standard fourth-order Runge-Kutta scheme. Winds and temperatures are interpolated linearly in time from once daily values to the trajectory time step (1/2 hour). Heating rates are recalculated every 3 hours using interpolated temperatures, and are interpolated linearly to the trajectory time step between calculations. Horizontal winds are from the UKMO data assimilation system [Swinbank and O'Neill 1994] and vertical velocities from a recent version of the middle atmosphere radiation code MIDRAD, an earlier version of which is described by Shine [1987]. Temperatures in the radiation code are from the UKMO data; MLS ozone is used in the heating rate calculation, except for the December 1993 case, when MLS ozone measurements are not continuously available. Manney et al. [1994b] discuss the impact of using climatological versus MLS ozone.

The temperatures shown here are from the UKMO data, and Rossby-Ertel potential vorticity (PV) calculated from the UKMO data [Manney and Zurek 1993] is also used.

MLS ozone data are available from September 1991 to the present. MLS H_20 and CLAES data are available through the 1992/1993 NH winter. Because of the UARS orbit, the data coverage switches from $\approx 34^{O}S$ to 80°N to $\approx 80^{O}S$ to 34°N approximate] y every 36 days. The examples examined here occur during late February and early March 1993, December 1992 and December 1993 in the NH, and in the 1993 and 1994 SH winters,

Observed Characteristics

Figure 1 shows maps of 840 K ozone, with wo PV contours overlaid, for three time periods in the NH winter. Stratospheric warmings during February and March 1993 were described by Manney et al. [1994a]; early winter warmings during December 1992 are described by Rosier et al. [1994] and during December 1993 by Manney et al. [1994c]. The PV contours shown on the ozone maps are in the region of strong gradients

coincident with the jet core, and thus approximately identify the edge of the polar vortex. In each of these time periods, tongues of relatively high ozone from low latitudes are drawn up around the polar vortex and into the region of the anticyclone which intensifies during stratospheric warmings (23 Feb 1993, 12 Dec 1992, 28 Nov 1993). In the succeeding days, however, an isolated region of low ozone forms in the anticyclone, with ozone mixing ratios comparable to those well within the polar vortex (7 Mar 1993, 24 Dec 1992, 18 Dec 1993). This region of low ozone may persist for some time, for example, the low ozone seen in the anticyclone on 7 Mar 1993 persists for over a week after that date, and mixing ratios become even lower.

Figure 2 displays the 840 K temperatures on the two days in Dec 1992, showing the typical relationship between the region of maximum temperatures and that of low ozone. In each of these events, the maximum temperatures are seen near the time when tongues of high ozone are being drawn up around the vortex, The region of lower ozone forms to the eastward and equatorward side (downstream) of the region of highest temperatures, several days after the temperature maximum.

Figure 3 shows the vertical structure of the pockets of low ozone, Profiles taken along the orbit tracks (i.e., prior to the gridding) are shown in the region of the low ozone anomaly on a day when it is well developed. The green profiles in Figs. 3b and c and the red profile in Fig. 3a are near the edge of the region, The pressure levels labeled are the levels at which MLS data are currently retrieved, In general, the anomaly appears as a bite out of the ozone profile in the altitude region of the mixing ratio peak, most prominent at the 10 hPa and 4.6 hPa retrieval levels. Ozone mixing ratios outside the vortex at these latitudes are typically near 8 ppmv [e.g., Froidevaux et al. 1994] even when higher ozone is not drawn up from low latitudes, so these anomalies represent a decrease in ozone that is in some cases over 3 ppmv. Similar features are also apparent in the CLAES ozone data during periods when they are available.

840 K N_2O maps for the February/March 1993 period [Manney et al. 1994a] show a tongue of high N_2O drawn into the anticyclone from low latitudes, and high N_2O persisting in the anticyclone through the period. Similar N_2O maps for the December 1992 period (not shown) again show high N_2O being drawn in from low latitudes, and Persisting in the anticyclone. 840 K maps of MLS H_2O for Dec 1992 [Manney et al. 1994c] and Feb/Mar 1993 (not shown) show a tongue of low H_2O drawn in from low latitudes persisting in the anticyclone during the time when low ozone appears. 'I'he behavior of these passive tracers suggests that low ozone in the anticyclone may not be expected to result from transport processes alone. However, this postulate requires further study since the different vertical and horizontal gradients of each of these trace species means that three-dimensional transport processes will affect each differently. In the next section, we examine in more detail the three-dimensional motion of air in the region of these anomalies.

Diagnosis of Air Motion

To examine the origin of the air with low ozone mixing ratios in the anticyclone, we have initialized a number of parcels (between 3200 and 3840 per level in each case) on several isentropic surfaces in the mid-stratosphere, in the region of low ozone, and run 22 day back trajectory calculations (back to near the beginning of the period when MLS began looking north). Figure 4 shows the initial positions of parcels started at 840 K, and their positions 20 days earlier for each of the 3 events. The parcels are color coded by the observed ozone at their positions on the plotted day. In each case, the trajectory calculation suggests that most or all of the parcels originated at lower latitudes in a region of much higher ozone than in the anomaly. In the December 1993 case, it can be seen that, as long as 20 days before the calculation was initialized, most of the parcels are grouped together in a fairly localized area. This event was the most persistent of those shown

here, but, in fact, examination of the other cases 10 days before the initialization (not shown) shows most of the parcels grouped together in a small region. Thus, the air in which the anomalies form appears to have been confined together for a week or more in each case. Very similar evolution is seen for parcels started at 740 K and 960 K.

Figure 5 shows the calculated potential temperatures of the parcels 20 days before the initialization. The trajectory calculation indicates that the parcels originated 60-140 K higher in potential temperature at that time, and thus experienced diabatic descent from ≈3 -7 K/d. The strongest diabatic descent rates during stratospheric warmings are in the region between the vortex and the anticyclone, coincident with the region of highest temperatures [e.g. Manney et al 1994a]. In moving up from low latitudes, and in circulating around the anticyclone, the parcels in the region of the ozone anomaly are among those that experience the strongest diabatic descent [Manney et al. 1994b].

Figure 6 summarizes the behavior of ozone at the parcel positions for the length of the back trajectory calculations, The average, minimum, and maximum observed ozone mixing ratios at the parcel positions are plotted as a function of time. The slopes for the averages shown in Fig. 6, calculated using a least squares fit over the 22 days, are given in Table 1. Ozone in each case decreases at an average rate of ≈ 1.5--2.O%/day for the ensemble of parcels, As an indication of the reliability of the three-dimensional trajectory calculation, the same calculation has been done for the Feb/Mar 1993 and December 1992 cases using MLS H_20, CLAES N_20, and CLAES CH_4. Figure 7 shows the results for N_20, and the least squares fits for each of the tracers are given in Table 1. The N_2O values for Feb/Mar 1993 show little trend (Fig. 7a), with the uncertainty being about half the magnitude of the slope; the slopes for the other passive tracers are also relatively small during this period. This is in contrast to the ozone (Fig. 6a), which shows a steady decreasing trend of ≈2%/d. The slopes for the tracers in December 1992 are again much smaller than those for ozone. The N_2O values for December 1992 show a greater trend than was apparent for Feb/Mar 1993 when averaged over the 22 day period. However,

most of the change occurs around 14-16 December (Fig. 7b); when the periods before and after this are fitted separately, the slopes for N_2O are only ≈0.3%/d, while those for ozone remain near 1.5%/d. 14-16 December is approximate] y the time before which the parcels split into two general groups (see Fig, 4d), and this may indicate a greater uncertainty in the trajectory calculations for days before=14 December.

The passive tracer calculations suggest that the trajectory code can fairly accurately reproduce the air motion. The behavior of the tracers is in contrast to the steady, consistent downward trend in ozone at the parcel positions in each case. In Feb/Mar 1993, the average ozone mixing ratio closely parallels the maximum; the low minimum values result from a few (on the order of 10 out of 3200) parcels that end up away from the others, as seen in Fig. 4b. In each case, the average value on the earliest day is greater than the maximum value on the initialization day.

Figure 8 shows the average of the ozone profiles at the horizontal postions of the parcels (the ozone profile is interpolated to each parcel's latitude and longitude, and then the values at each level are averaged) as a function of potential temperature on each day of the trajectory calculations. The average potential temperature of the ensemble of parcels that started at 840 K is also indicated. At the end of the back trajectory calculation, mixing ratios as low at those at the initial (latest day) parcel potential temperature are seen only several hundred Kelvin above or below the parcel potential temperature. This indicates that the calculated potential temperature would have to be in error by several hundred Kelvin in order to obtain the observed mixing ratio by vertical transport, if the average calculated horizontal motion is accurate. An error of this magnitude is not expected in the radiation calculation for the mid-stratosphere, and if present would also have been reflected in passive tracers trends, since each of the tracers examined has a strong vertical gradient,

The results in this section indicate that the observed pockets of low ozone in the mid-stratospheric anticyclone could not result from transport processes alone.

Discussion

Three examples are shown of the formation of an isolated region of low ozone mixing ratios in the NH anticyclone during strong stratospheric warmings. These examples are typical of the ozone behavior in the mid-stratosphere when a strong anticyclone develops. In addition to the examples given here, a similar pocket of low ozone forms in the anticyclone during every strong NH warming observed by MLS. Since SH warmings are generally much weaker than in the NH, and any SH anticyclone that forms is usually a very transient feature, examples of this type of behavior are less apparent in the SH. However, Figure 9 shows 840 K SH ozone on 22 Aug 1993, and on 30 May 1994, each a few days after the peak of a SH warming, when an anticyclone had formed. There is a suggestion of a region of low ozone in the anticyclone on 22 Aug 1993, and a distinct region of low ozone in the anticyclone on 30 May 1994. Vertical profiles in these regions (Fig. 10) show a bite out of the profiles similar to, but smaller than, those seen in the NH. 30 May 1994 is only a few days after MLS began observing the SH, so no back trajectories were computed for this case. Figure 11 shows observed ozone at parcel positions on 22 Aug 1993 (the initial day) and 13 days earlier (the first day MLS was looking south), While not as dramatic as the NH examples, the calculation does show the parcels originating from low latitude regions of higher ozone, and average ozone at the parcel positions decreases at =1%/d over the period. An analysis similar to that shown in Fig. 8 suggests that the calculated vertical position of the parcels would have to be in error by ≈100 K in potential temperature over the 14 days in order to produce the observed ozone on 22 Aug solely by transport processes. Thus, the same phenomenon described for the NH does in fact occur in the SH when the anticyclone becomes sufficiently strong and persistent.

Although the anomalously low ozone in the anticyclone has not been previously studied in detail, the phenomenon is apparent in mid-stratospheric Limb Infrared Monitor

of the Stratosphere (LIMS) data shown by Leovy et al, [1985]. Figure 12 Shows 840 K LIMS ozone on 23 January 1979, during a strong warming. A low ozone anomaly similar to those studied here is apparent in the anticyclone. This bite out of the LIMS ozone profiles extends vertically from ≈20 to 7 hPa. It appears that this feature may not be as intense as some of those seen in MLS observations, but the separation of over a decade between the two datasets, and the limited length of the LIMS dataset render such comparisons speculative.

Rood et al. [1993] noted an anomaly in LTMS nitric acid (HNO_3) in late January 1979, with high HNO_3 values, comparable to those in the polar vortex, in a isolated region in the anticyclone. This feature was seen over a vertical range from ≈30 to 5 hPa. The ozone anomaly shown in Fig. 12 is nearly coincident in the horizontal with the $HN0_3$ anomaly reported by Rood et al. [1993], but is apparent only between ≈20 and 7 hPa. The $HN0_3$ anomaly is slightly downstream of the ozone anomaly. Examination of CLAES HNO_3 data during Feb/Mar 1993 and December 1992 indicates that at those times there is also a region of high $HN0_3$ just downstream of the region of low ozone. High $HN0_3$ in the anticyclone was also observed by the Improved Stratospheric and Mesospheric Sounder (ISAMS) during the January 1992 nearly major stratospheric warming, when MLS also observed a pocket of low ozone [J. Remedies, paper in preparation]. Rood et al. [1993] were unable to reproduce the $HN0_3$ anomaly observed in LIMS data using a three-dimensional chemical-transport model, and concluded on that basis that there must either be serious flaws in the data, or deficiencies in the chemical model, Recent independent data suggest that this phenomenon is in fact a real atmospheric feature, and that it is related to the low ozone anomalies described here. Work is now in progress by several groups with the goal of reproducing these phenomena in chemical models.

Conclusions

MLS observations of the evolution of mid-stratospheric ozone during stratospheric warmings have been examined during the past three winters in each hemisphere, During warmings, tongues of high ozone are drawn up from low latitudes into the developing anticyclone. Several days later, an isolated region of low ozone mixing ratios appears, centered in the anticyclone, and prominent at MLS retrieval levels of 10 and 4.6 hPa. Ozone mixing ratios in this region during NH warmings are comparable to values well inside the vortex, and are typically ≈3 ppmv lower than typical mid-latitude extra-vortex mixing ratios. This type of feature appears whenever the anticyclone is strong and persistent, including during relatively strong minor warmings in the SH.

Three-dimensional trajectory calculations shown here indicate that the air in the region where the low ozone anomalies form originates at higher altitudes and low latitudes, where ozone mixing ratios are much higher than those in the anomaly. The air parcels studied here are typically confined together for 1 to 3 weeks before the lowest ozone mixing ratios are observed. Comparison with passive tracer data shows that the trajectory calculation used here can fairly accurately reproduce observed air motions. This, and the extremely large magnitude of the errors that would be implied in the trajectory calculation to get observed ozone values by transport, confirms that the observed ozone anomalies in the mid-stratosphere could not result solely from transport processes.

Several modeling investigations are underway aimed at understanding the chemical processes involved in the formation of these anomalies. The following summarizes the features that must be explained by combined chemical and dynamical models:

- Low ozone appears in the anticyclone several days after the peak of a stratospheric warming,
- The ozone anomaly extends from ≈15 to 5 hPa in the vertical, with higher ozone above and below.

- The region of low ozone is downstream (eastward and equatorward) of the region of maximum temperature.
- The air in which the anomaly forms originates at low latitudes and higher altitudes, in regions of much higher ozone.
- This air remains localized together for 1 to 3 weeks prior to the appearance of minimum ozone mixing ratios.
- Anomalies in HNO_3 [Rood et al. 1993] and possibly other species [J, Remedies, paper in preparation] are observed concurrently.

Acknowledgments. Thanks to our MLS and CLAES colleagues for their contributions to its success; to B. Ridenoure for data analysis and graphics assistance, to T, Luu for data management, to P. Newman for supplying routines that were adapted to calculate PV. The UARS investigations at the Jet Propulsion Laboratoy, California Institute of Technology were carried out under contract with the National Aeronautics and Space Administration.

References

Andrews, D. G., J. R. Holton, and C. B. Leovy, *Middle Atmosphere Dynamics.* Academic Press, New York, 489pp, 1987.

Barath, F. T., M. C. Chavez, R, E, Cofield, D. A, Flower, M. A, Frerking, M. B. Gram, W. M. Harris, J. R. Holden, R. F. Jarnot, W. G, Kloezeman, G. J. Klose, G. K, Lau, M. S. Loo, B. J. Maddison, R. J. Mattauch, R. P. McKinney, G. E. Peckham, H. M. Pickett, G. Siebes, F. S. Soltis, R. A. Suttie, J. A. Tarsala, J. W. Waters, and W. J. Wilson, The Upper Atmosphere Research Satellite Microwave Limb Sounder instrument, *J. Geophys. Res.*, **98,** 10,751-10,762, 1993.

Elson, L. S., and L. Froidevaux, The use of Fourier transforms for asynoptic mapping: Early results from the Upper Atmosphere research Satellite Microwave Limb Sounder, *J. Geophys. Res.,* 98,23,039-23,049, 1993.

Farrara, J. D., M. Fisher, C. R. Mechoso, and A. O'Neill, Planetary-scale disturbances in the southern stratosphere during early winter. *J. Atmos. Sci.*, **49, 1757-1775, 1992.**

Fishbein, E. F., L. S. Elson. L. Froidevaux, G. L. Manney, W. G. Read, J, W. Waters, and R. W. Zurek, MLS observations of stratospheric waves in temperature and O_3 during the 1992 southern winter. *Geophys. Res. Lett.,* 20, 1255-1258, 1993,

Froidevaux, L., J. W. Waters, W. G. Read, L. S. Elson, D. A. Flower, and R. F. Jarnot, Global ozone observations from UARS MLS: An overview of zonal mean results. *J. Atmos. Sci.,* in press, **1994.**

Kumer, J. B., J. L. Mergenthaler, and A. E. Roche, CLAES CH_4, N_20, and CCL_2F_2 (FI 2) global data, *Geophys. Res. Lett.,* 20,1239-1242,1993.

Lahoz, W. A., A. O'Neill, E, S, Carr, R, S. Harwood, L, Froidevaux, W. G, Read, J. W. Waters, J, B. Kumer, J. L. Mergenthaler, A, E, Roche, G. E. Peckham, and R. Swinbank, Three-dimensional evolution of water vapour distributions in the northern

hemisphere as observed by MLS. *J. Atmos. Sci.,* in press, 1994.

Leovy, C. B., C.-R. Sun, M. H. Hitchman, E, E, Remsberg, J. M. Russell III, L, L. Gordley, J. C. Gille, and L. V. Lyjak, Transport of ozone in the middle stratosphere: Evidence for planetary wave breaking. *J. Atmos. Sci.,* 42,230-244, 1985.

Manney, G. L., J. D. Farrara, and C. R. Mechoso, The behavior of wave 2 in the Southern Hemisphere stratosphere during late winter and early spring. *J. Atmos. Sci.,* **48, 976-998,** 1991.

Manney, G. L., and R, W. Zurek, Interhemispheric Comparison of the development of the stratospheric polar vortex during fall: A 3-dimensional perspective for 1991-1992, *Geophys. Res. Lett.,* 20, 1275-1278, 1993.

Manney, G. L., L. Froidevaux, J. W. Waters, L. S. Elson, E. F. Fishbein, R, W. Zurek, R. S. Harwood, and W. A, Lahoz, The evolution of ozone observed by UARS MLS in the 1992 **late winter southern polar vortex,** *Geophys. Res. Lett.,* 20, 1279-1282, 1993.

Manney, G. L., R, W. Zurek, A, O'Neill, R. Swinbank, J. B. Kumer, J. L, Mergenthaler, and A. E. Roche, Stratospheric Warmings during February and March 1993. *Geophys. Res. Lett.,* **21,813-816, 1994a,**

Manney, G. L., R. W. Zurek, A, O'Neill, and R. Swinbank, On the motion of air through the stratospheric polar vortex, *J. Atmos. Sci.,* in press, 1994b.

Manney, G. L., W. A. Lahoz, L. S. Elson, L, Froidevaux, R. S. Harwood, A. O'Neill, R, Swinbank, J. W. Waters, and R. W. Zurek, 1994b: Stratospheric warmings during earl y winter in the Northern and Southern Hemispheres, Q. *J. Roy. Met. Sot.,* submitted, 1 994c.

Roche, A. E., J. B. Kumer, J. L. Mergenthaler, G. A, Ely, W. G, Uplinger, J. F. Potter, T. C. James, and L. W. Sterritt, The Cryogenic Limb Arrary Etalon Spectrometer (CLAES) on UARS: experiment description and performance, *J. Geophys. Res.,* 98,

10,763-10,775, 1993.

Rood, R. B., A. R. Douglass, J. A. Kaye, and D. B. Considine, Characteristics of winter-time and autumn nitric acid chemistry as defined by Limb Infrared Monitor of the Stratosphere (LIMS) data, *J. Geophys. Res.*, 98, 18,533-18,545, 1993.

Rosier, S. M., B. N. Lawrence, D. G. Andrews, and F. W. Taylor, Dynamical evolution of the northern stratosphere in early winter 1991-92, as observed by the Improved Stratospheric and Mesospheric Sounder, *J. Atmos. Sci.*, in press, 1994.

Shine, K. P., The middle atmosphere in the absence of dynamic heat fluxes. *Quart. J. Roy. Meteor. Sot.*, **113,603-633, 1987.**

Swinbank, R., and A. O'Neill, 1994: A Stratosphere-troposphere data assimilation system. *Mon. Wea. Rev., 122,686-702.*

Waters, J. W., "Microwave Limb Sounding", in *Atmospheric Remote Sensing by Microwave Radiometry,* Ed: M. A. Janssen, 383-496, 1993.

Waters, J. W., L. Froidevaux, W. G. Read, G. L, Manney, L, S, Elson, D. A. Flower, R. F. Jarnot, and R. S. Harwood, Stratospheric C1O and ozone from the Microwave Limb Sounder on the Upper Atmosphere Research Satellite, *Nature, 362,597-602,* 1993a.

Table 1. Time rates of change of average ozone, N_2O, CH_4, and H_2O at positions of parcels started at 840 K, calculated using a linear least square fit over the 22 day back trajectory calculation. Approximate change in percent per day is given in parentheses with each value.

Time Period	$\Delta O_3/\Delta t$ (ppmv/day)	$\Delta N_2O/\Delta t$ (ppbv/day)	$\Delta CH_4/\Delta t$ (ppmv/day)	$\Delta H_2O/\Delta t$ (ppmv/day)
Feb/Mar 1993	-0.152 ± 0.006 (-2.3%/d)	-0.44 ± 0.22) (-0.4%/d)	-0.010 ± 0.003 (-0.8%/d)	-0.31 ± 0.004 (-0.6%/d)
Dec 1992	-0.086 ± 0.003 (-1.5%/d)	0.51 ± 0.10 (0.6%/d)	-0.006 ± 0.002 (-0.5%/d)	-0.31 ± 0.002 (-0.6%/d)
Dec 1993	-0.088 ± 0.002 (-1.5%/d)			

Figure Captions

Figure 1. Synoptic maps of ozone mixing ratios (ppmv) with overlaid PV contours at 840 K, in the NH, on (a) 23 Feb 1993, (b) 7 Mar 1993, (c) 12 Dec 1992, (d) 24 Dec 1992, (e) 28 Nov 1993 and (f) 18 Dec 1993. Overlaid PV contours at 840 K are 3.0 and 5.0 x 10^{-4} K m^2 kg^{-1} s^{-1}. Projection is orthographic, with 0° longitude at the bottom of the plot, and 30 and 60° latitude circles shown as thin dashed lines.

Figure 2. Synoptic maps of UKMO temperatures at 840 K in the NH on (a) 12 Dec 1992 and (b) 24 Dec 1992. Layout is as in Fig, 1.

Figure 3. Individual MLS ozone profiles on (a) 8 Mar 1993, (b) 24 Dec 1992 and (c) 16 Dec 1993, in the region of the ozone anomaly,

Figure 4. Initial horizontal positions of parcels started at 840 K on (a) 7 Mar 1993, (c)24 Dec 1992 and (e) 18 Dec 1993, and the positions of those parcels 20 days previously (b, d, and f). Parcels are color coded by the observed ozone value at their position on the plotted day. Projection is orthographic, with 0° longitude at the bottom of the plot, and 30 and 60° latitude circles shown as thin dashed lines,

Figure 5. As is Fig. 4, for 20 days prior to initialization only, and with parcels color coded by their potential temperature.

Figure 6, Average (circles), minimum (triangles) and maximum (squares) ozone mixing ratio (ppmv) at parcel positions on each day of the back trajectory calculation, for (a) Feb/Mar 1993, (b) Dec 1992 and (c) Dec 1993. (a) and (b) are averaged over 3200 parcels, (c) over 3840 parcels,

Figure 7. As in Figure 6, but for N_20 mixing ratio (ppbv), and for (a) Feb/Mar 1993 and (b) Dec 1992 only.

Figure 8. Average ozone (ppmv) profile at horizontal positions of parcels initialized at 840 K. Ozone is interpolated to each parcel's latitude and longitude at each level

and then the profiles are averaged. For (a) Feb/Mar 1993, (b) Dec 1992 and (c) Dec 1993.

Figure 9. As in Fig. 1, but for the SH on (a) 22 Aug 1993 and (b) 30 May 1994, and with 0° longitude at the top of the plots. PV contours are -3.0 and -5.0x 10^{-4} K m^2 kg^{-1} s^{-1}.

Figure 10. As in Fig. 3, but for (a) 22 Aug 1993 and (b) 30 May 1994 in the SH.

Figure 11. As in Fig. 4, but for a back trajectory run started 22 Aug 1993 in the SH, on the initial day and 13 days previously. 0° longitude is at the top of the plots.

Figure 12. As in Fig. 1, but for 23 Jan 1979, from LIMS data,

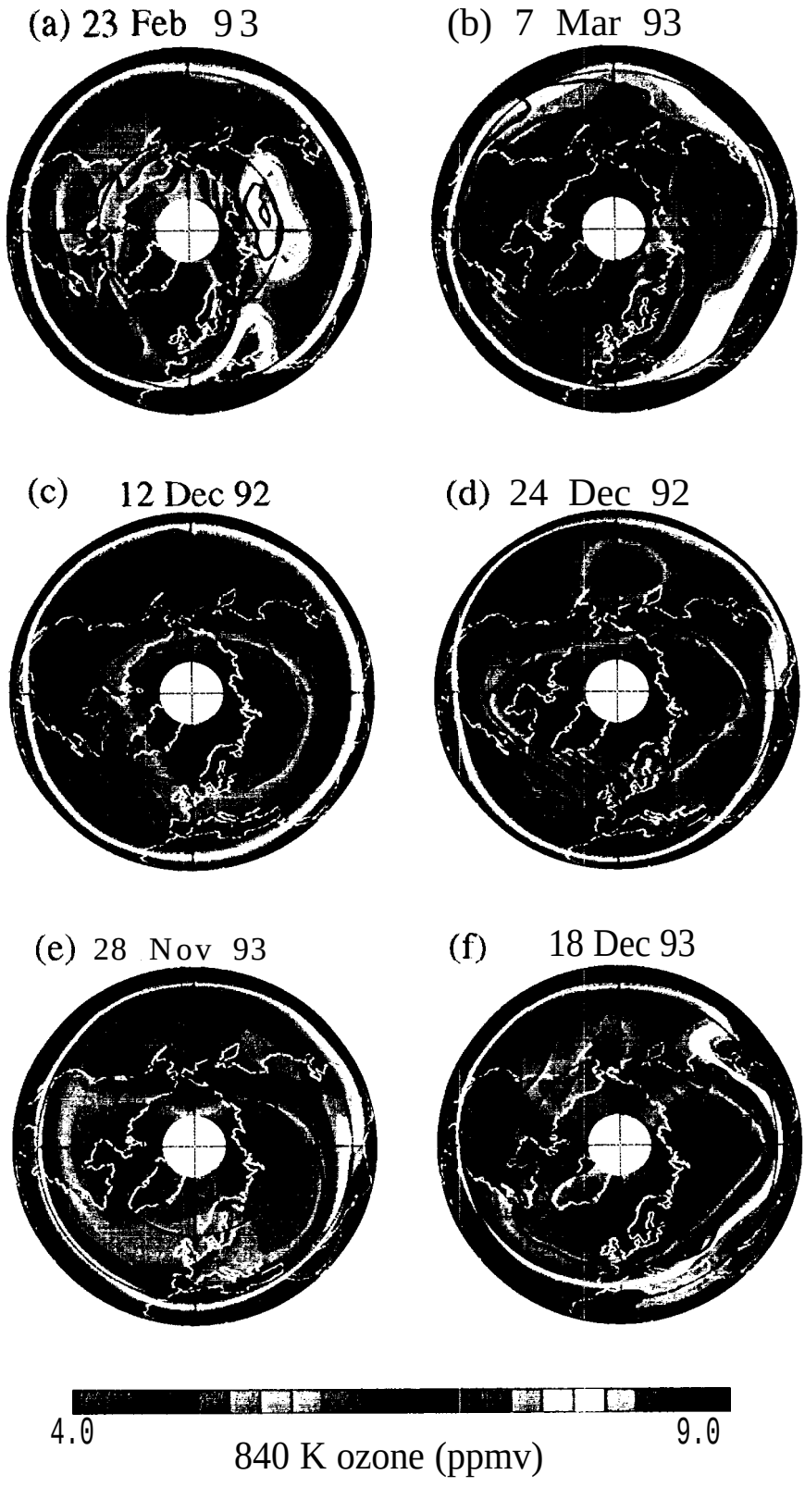
(a) 23 Feb 93
(b) 7 Mar 93
(c) 12 Dec 92
(d) 24 Dec 92
(e) 28 Nov 93
(f) 18 Dec 93
4.0
9.0
840 K ozone (ppmv)

Fig. 1

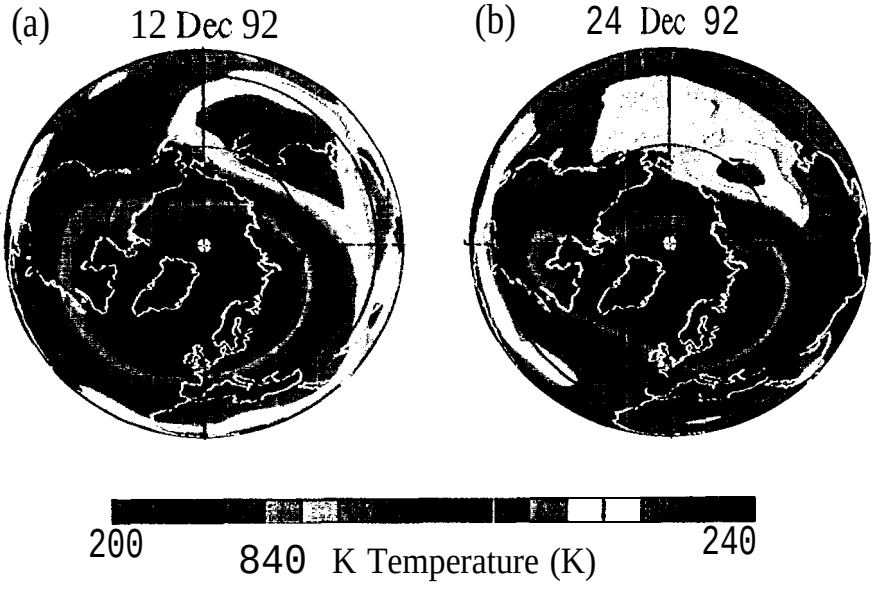

Fig. 2

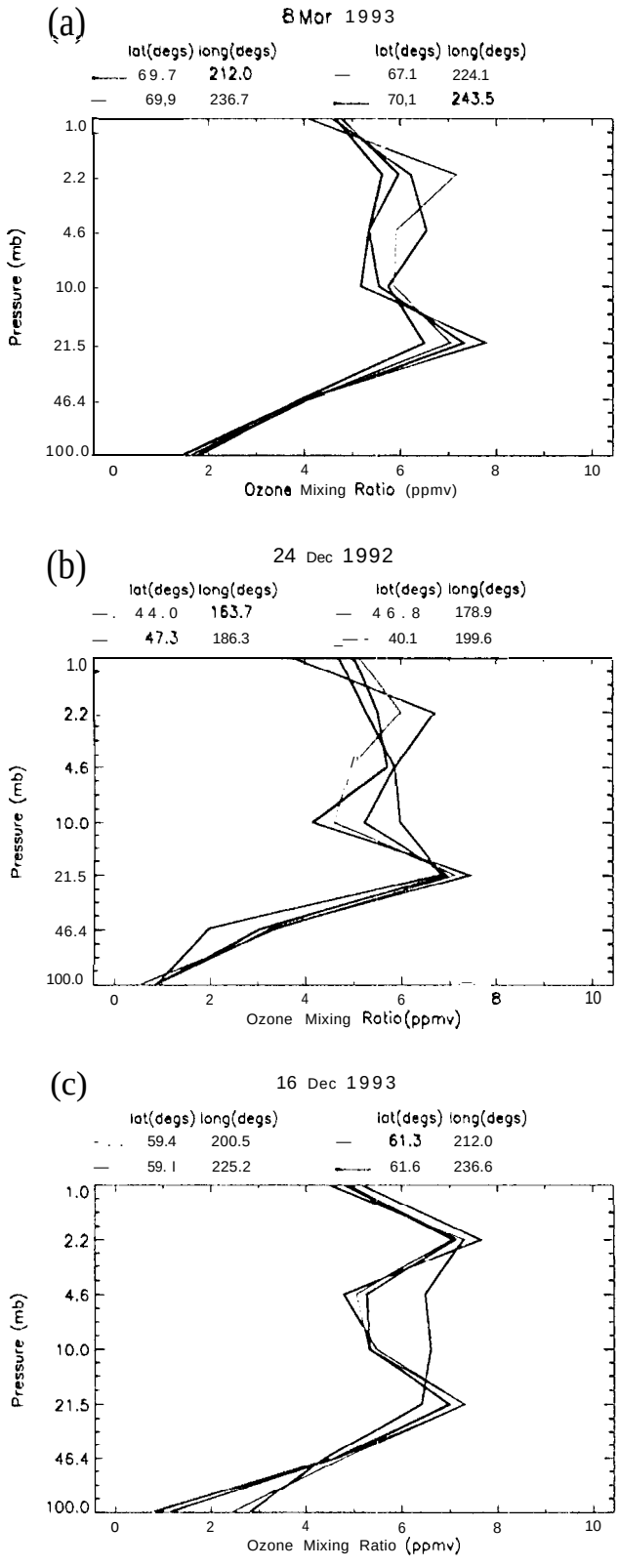
(a)
8 Mar 1993
lat(degs) long(degs)
69.7 212.0
69,9 236.7
lat(degs) long(degs)
67.1 224.1
70,1 243.5
Pressure (mb)
1.0
2.2
4.6
10.0
21.5
46.4
100.0
0
2
4
6
8
10
Ozone Mixing Ratio (ppmv)
(b)
24 Dec 1992
lat(degs) long(degs)
44.0 163.7
47.3 186.3
lat(degs) long(degs)
46.8 178.9
40.1 199.6
Pressure (mb)
Ozone Mixing Ratio (ppmv)
(c)
16 Dec 1993
lat(degs) long(degs)
59.4 200.5
59.1 225.2
lat(degs) long(degs)
61.3 212.0
61.6 236.6
Pressure (mb)
Ozone Mixing Ratio (ppmv)

Fig. 3

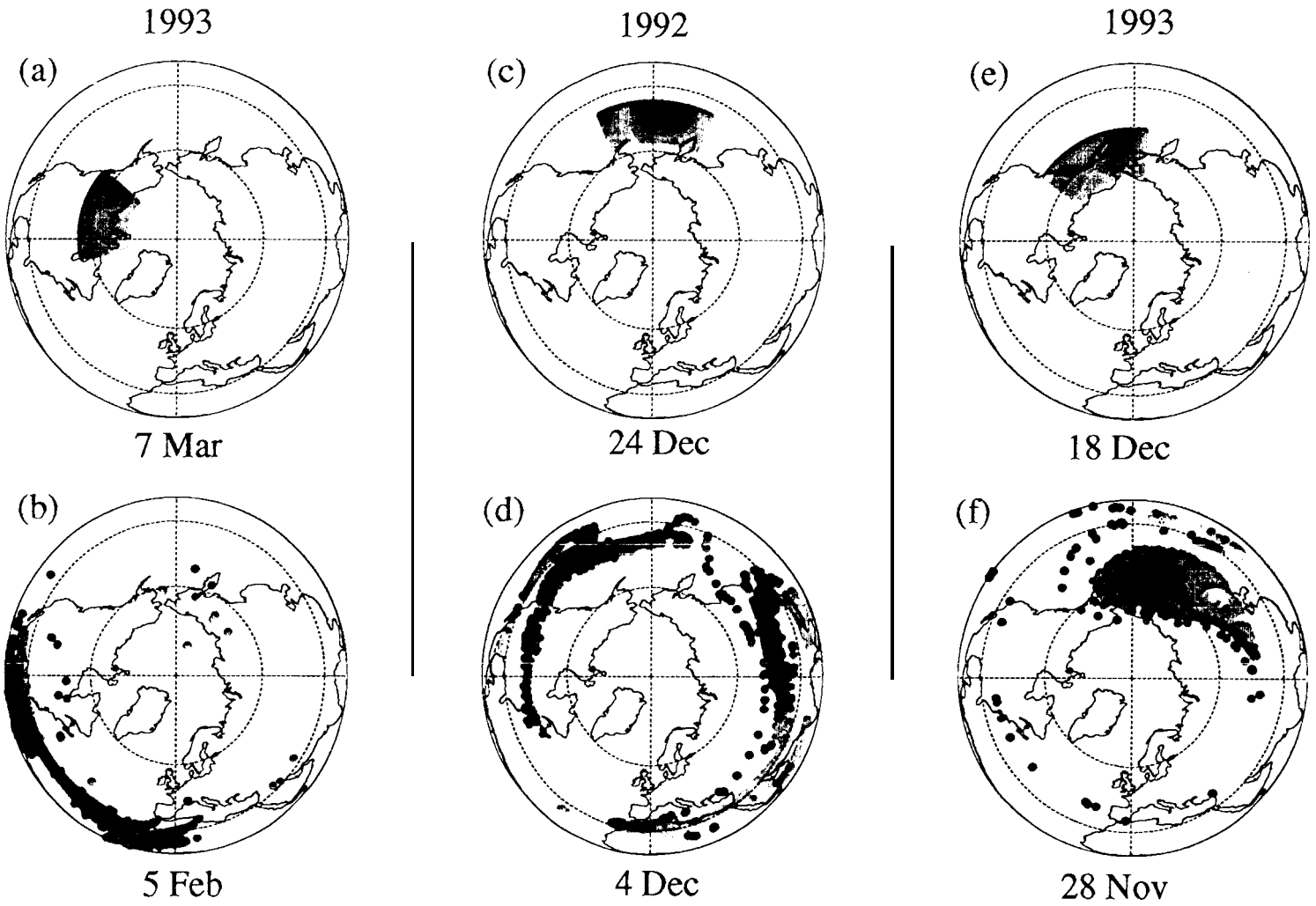

4 9

Fig. 4

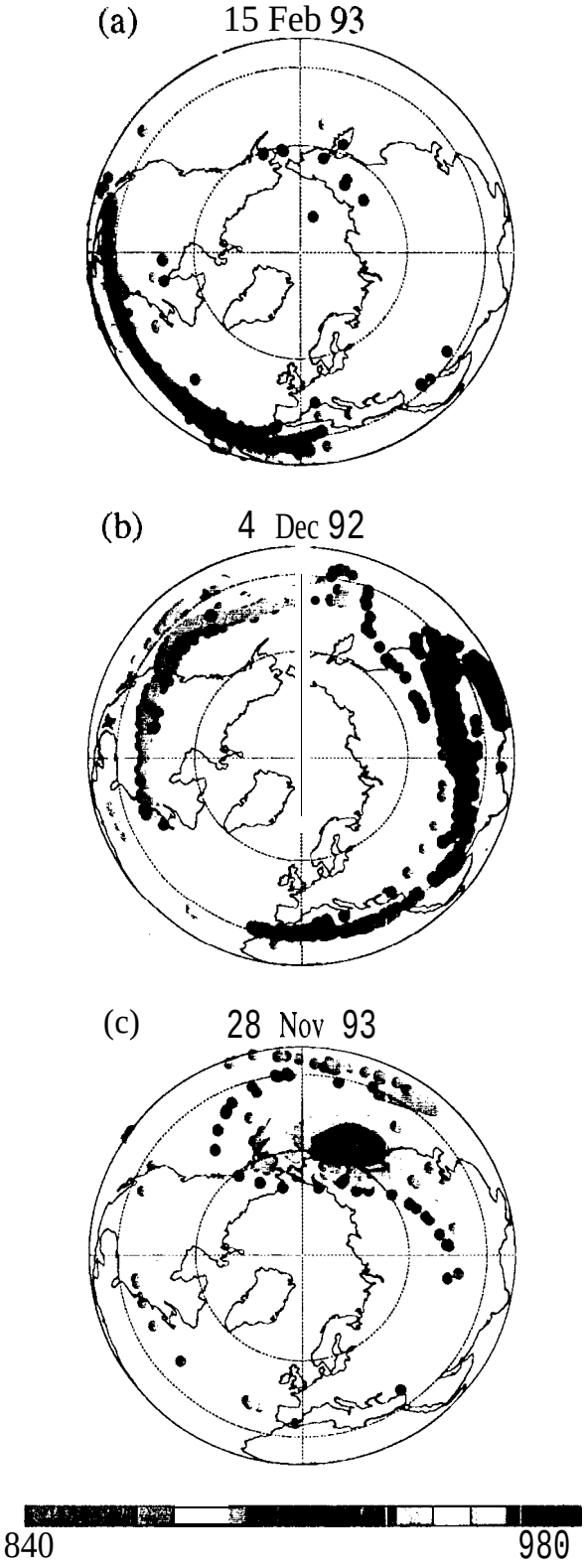

Fig. 5

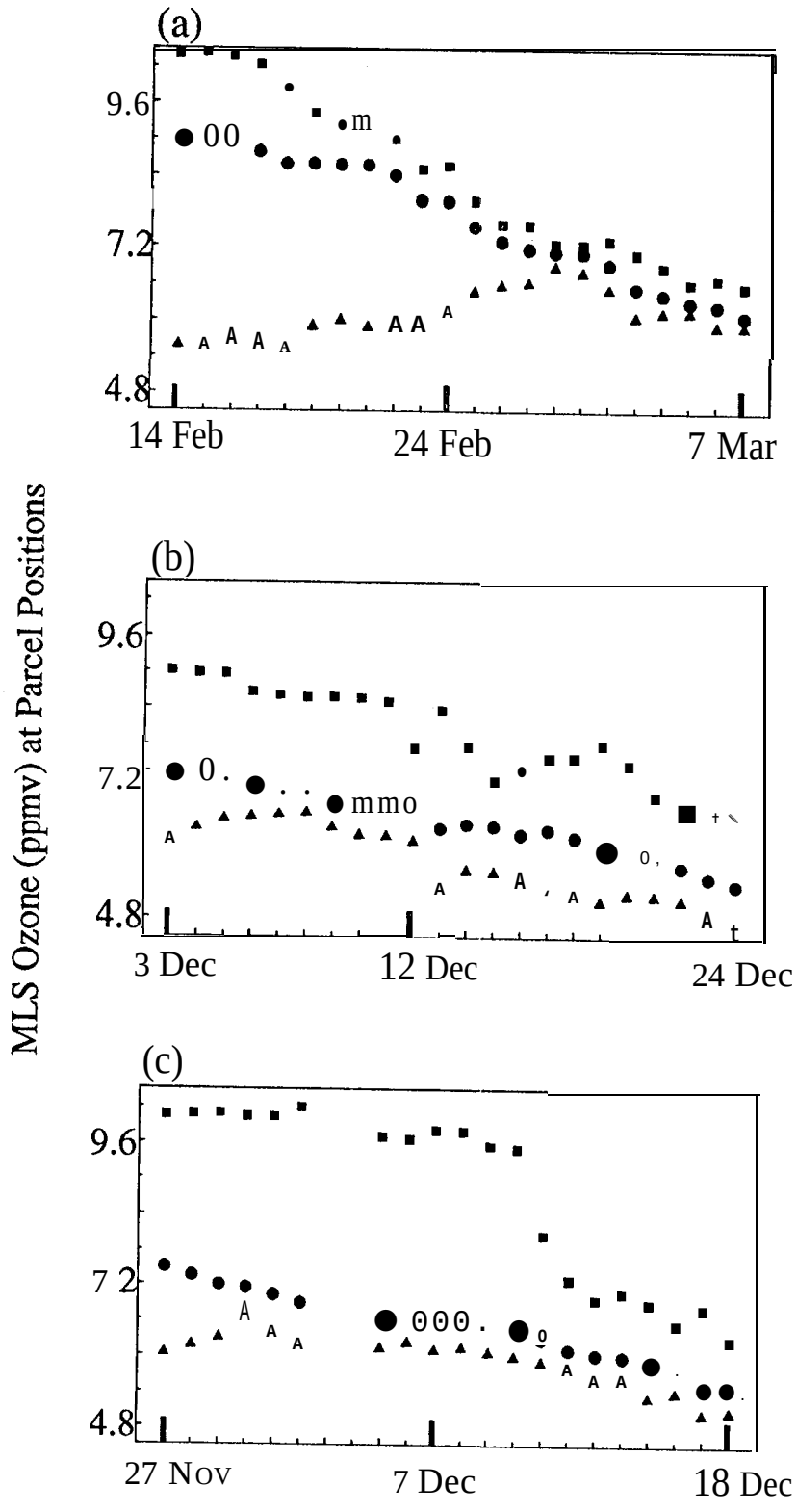
(a)
9.6
7.2
4.8
14 Feb
24 Feb
7 Mar
(b)
9.6
7.2
4.8
3 Dec
12 Dec
24 Dec
(c)
9.6
7 2
4.8
27 Nov
7 Dec
18 Dec
MLS Ozone (ppmv) at Parcel Positions

Fig. 6

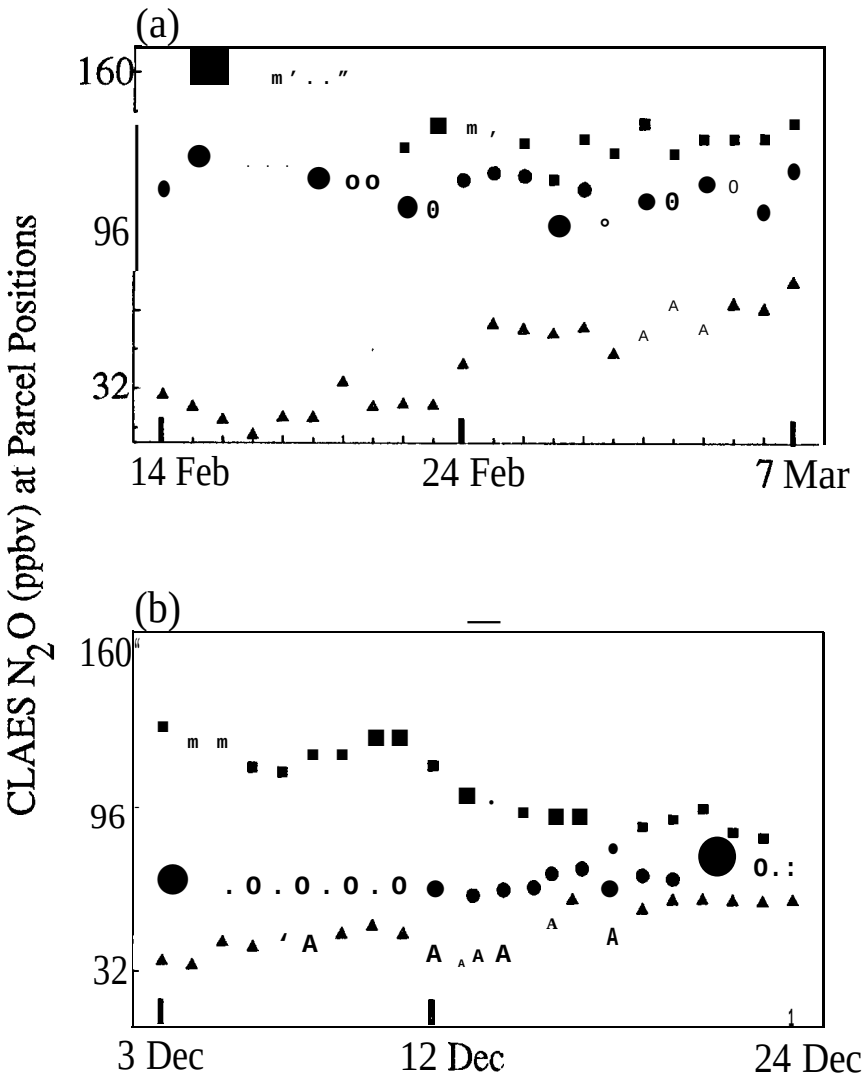
(a)
160
96
32
14 Feb
24 Feb
7 Mar
(b)
160
96
32
3 Dec
12 Dec
24 Dec
CLAES N_2O (ppbv) at Parcel Positions

Fig. 7

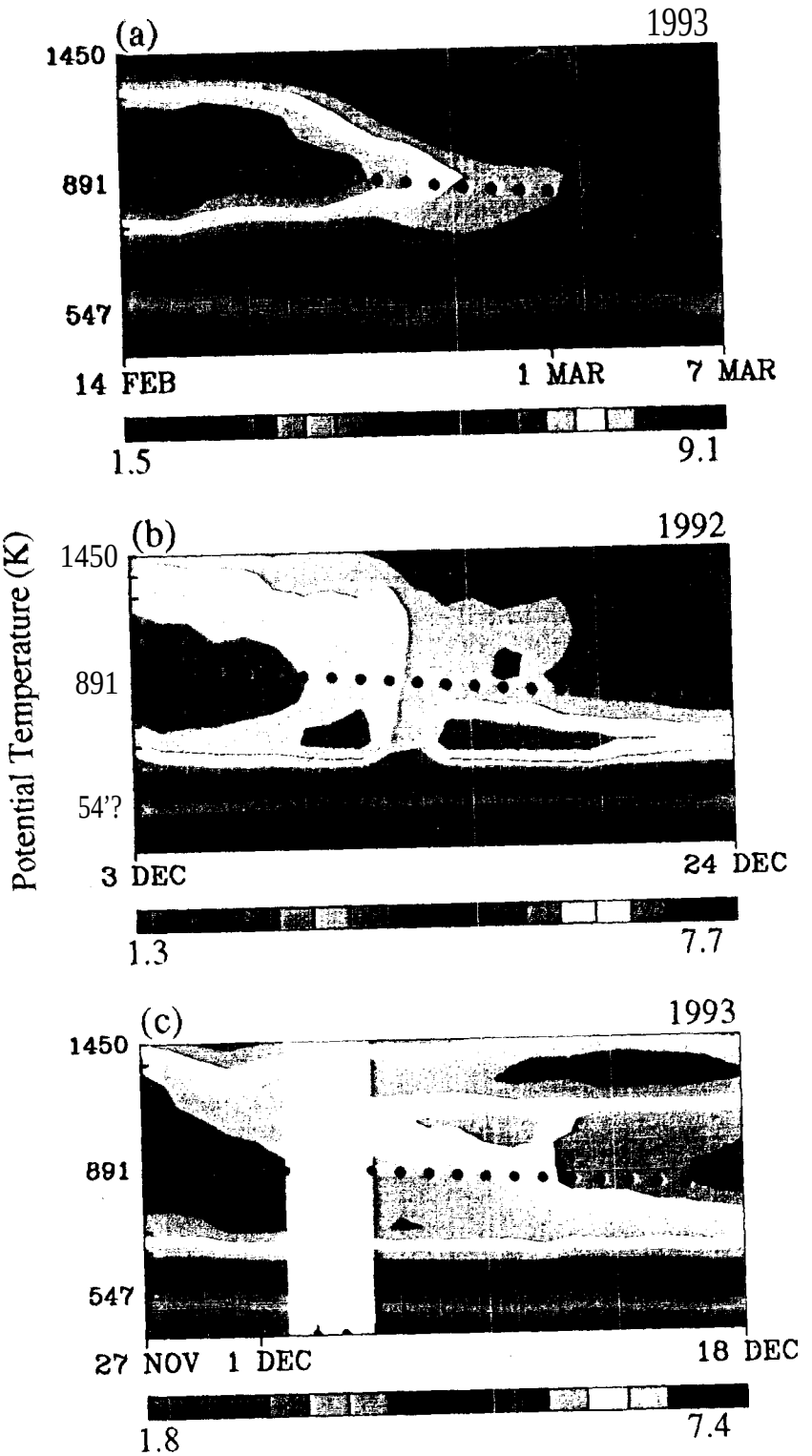
(a)
1993
1450
891
547
14 FEB
1 MAR
7 MAR
1.5
9.1
(b)
1992
1450
891
54'?
3 DEC
24 DEC
1.3
7.7
Potential Temperature (K)
(c)
1993
1450
891
547
27 NOV
1 DEC
18 DEC
1.8
7.4

Fig. 8

(a) 22 Aug 93

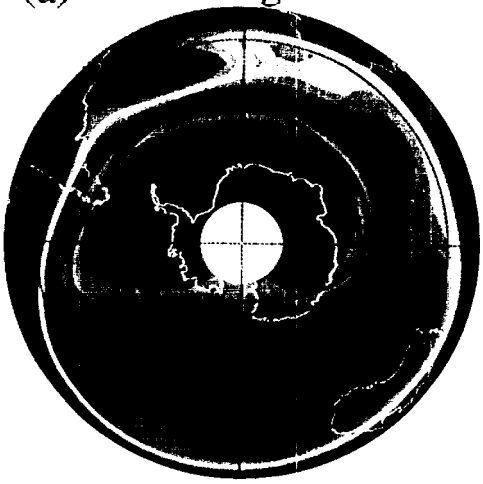

(b) 30 May 94

Fig. 9

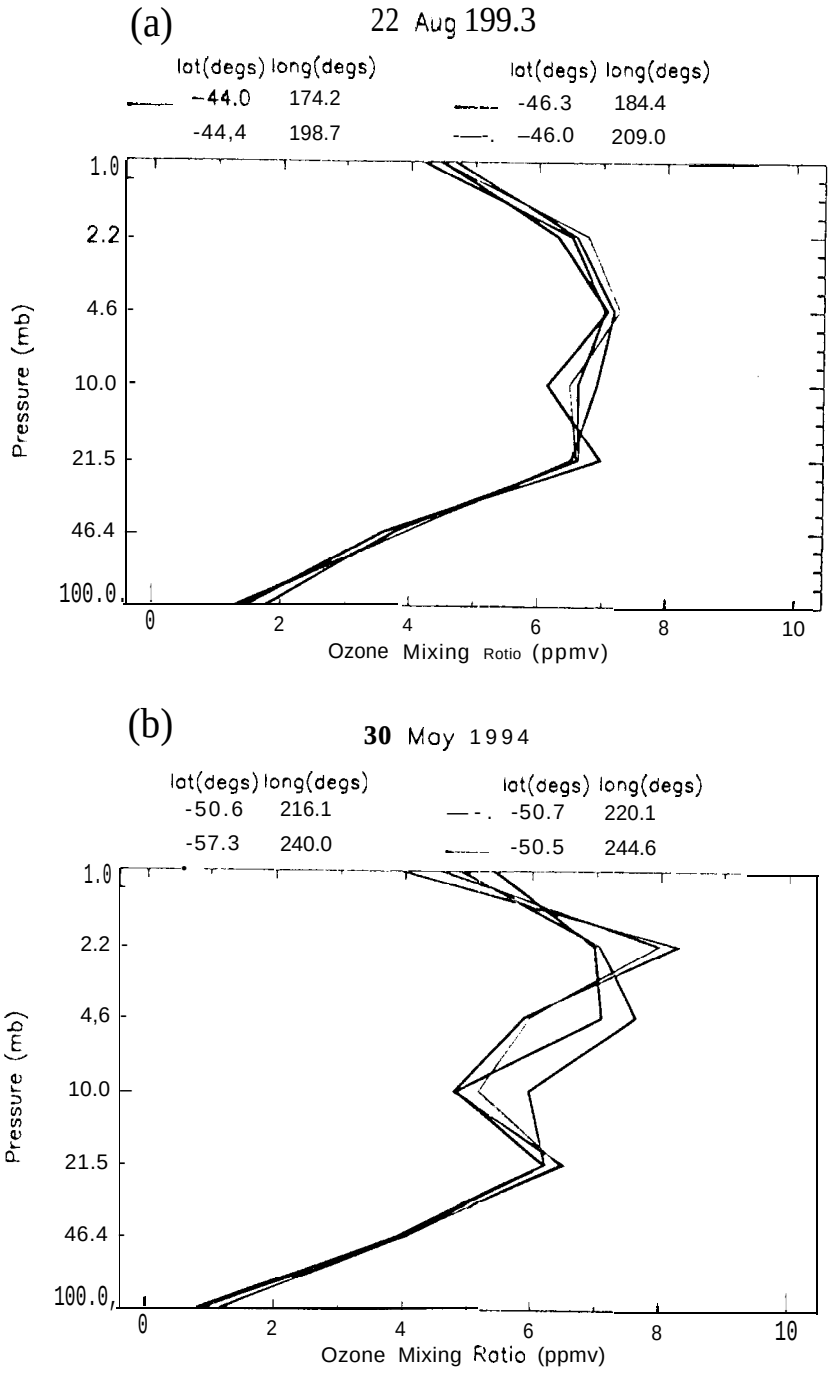
(a)
22 Aug 199.3
lat(degs) long(degs)
-44.0 174.2
-44,4 198.7
lat(degs) long(degs)
-46.3 184.4
-46.0 209.0
Pressure (mb)
1.0
2.2
4.6
10.0
21.5
46.4
100.0
0
2
4
6
8
10
Ozone Mixing Rotio (ppmv)
(b)
30 May 1994
lat(degs) long(degs)
-50.6 216.1
-57.3 240.0
lat(degs) long(degs)
-50.7 220.1
-50.5 244.6
Pressure (mb)
1.0
2.2
4,6
10.0
21.5
46.4
100.0
0
2
4
6
8
10
Ozone Mixing Ratio (ppmv)

Fig. 10

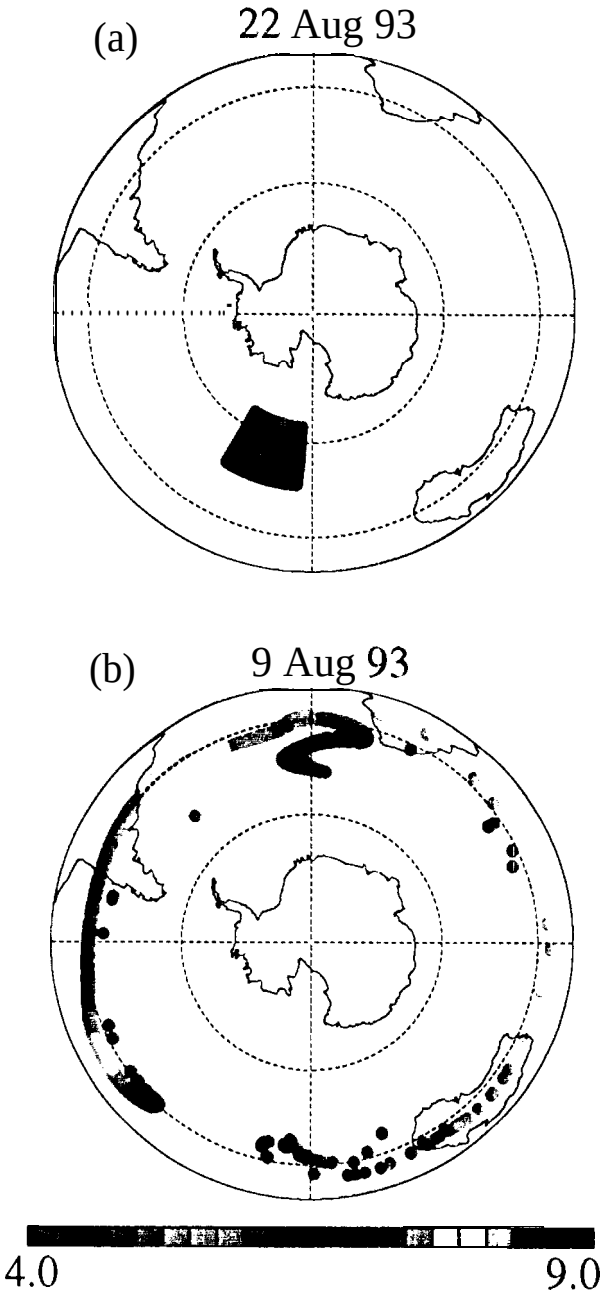

Fig. 11

23 Jan 79

4.0 9.0

Fig. 12